

Study of Microscale Three-Dimensional Printing Using Near-Field Melt Electrospinning

Xiangyu You

Department of Mechanical and Automation Engineering,
The Chinese University of Hong Kong,
Hong Kong, China

Chengcong Ye

Department of Mechanical and Automation Engineering,
The Chinese University of Hong Kong,
Hong Kong, China

Ping Guo¹

Mem. ASME
Department of Mechanical and Automation Engineering,
The Chinese University of Hong Kong,
Hong Kong, China
e-mail: pguo@mae.cuhk.edu.hk

Three-dimensional (3D) printing of microscale structures with high-resolution (submicron) and low-cost is still a challenging work for the existing 3D printing techniques. Here, we report a direct writing process via near-field melt electrospinning (NFME) to achieve microscale printing of single filament wall structures. The process allows continuous direct writing due to the linear and stable jet trajectory in the electric near field. The layer-by-layer stacking of fibers, or self-assembly effect, is attributed to the attraction force from the molten deposited fibers and accumulated negative charges. We demonstrated successful printing of various 3D thin-wall structures with a minimal wall thickness less than 5 μm . By optimizing the process parameters of NFME, ultrafine poly (ϵ -caprolactone) (PCL) fibers have been stably generated and precisely stacked and fused into 3D thin-wall structures with an aspect ratio of more than 60. It is envisioned that the NFME can be transformed into a viable high-resolution and low-cost microscale 3D printing technology. [DOI: 10.1115/1.4037788]

Keywords: 3D printing, near-field electrospinning, melt electrospinning

Introduction

Three-dimensional (3D) printing has recently been drawing a great amount of attention for fabricating thin-wall structures, which have been applied in numerous applications such as micro-electromechanical systems, biomedical sensors, microbatteries, and tissue engineering scaffolds [1–4]. For example, Sun et al. [3] demonstrated a 3D printed microscale thin-wall electrode architecture, which has doubled the energy density by fully utilizing the limited space available. Many novel techniques have been developed to achieve microscale thin-wall structures including selective laser sintering, stereolithography, selective laser melting, directed metal deposition, fused deposition modeling, inkjet printing, etc. [5–10]. These existing additive manufacturing processes, however, have intrinsic limitations when building microscale slender thin-wall structures. For instance, in a laser-based direct writing process, the minimal feature size is limited at 20 μm due to the laser spot size, powder diameter, thermal diffusion, etc. Fused deposition modeling is the least expensive direct writing approach, which has been widely adopted. The minimal feature size, however, is limited by the molten filament diameter in the range between 100 and 500 μm . For droplet-based printing processes, the resolution is limited by the nozzle diameter in the range of 20–50 μm . Furthermore, the small nozzle diameter requires extremely high injection pressure, which deteriorates its controllability. Hence, three-dimensional printing of microscale thin-wall structures with high-resolution and low-cost remains a challenging task, which motivates this paper.

Direct writing based on electrospinning is an attractive and viable approach to fabricate high-resolution microscale two-dimensional patterns, in which a dielectric liquid is subjected to a strong external electric field to form a Taylor cone with a fine jet emitted. Then, the electrospun nanofibers are collected as patterns by controlling the collector movement according to a user-defined program. It has been proved to be a high efficient and low-cost method to fabricate nanofibers. Based on the polymer used, electrospinning can be divided into solvent-based and melt-based

processes. Traditionally, solvent-based electrospinning is generally not considered as an additive manufacturing approach [11]. Most of the related works are limited to the two-dimensional pattern generation. Major difficulties of utilizing solvent-based electrospinning for additive manufacturing come from the jet bending instability and coulombic repulsion force of deposited fibers. There were some attempts to fabricate 3D microscale thin-wall structures via solvent-based electrospinning, using approaches such as prestructured substrates [12] and near-field electrospinning [13]. Lee and Kim [12] proposed a method to fabricate a freestanding straight wall by repetitive deposition of electrospun polymer nanofibers using a conducting line as the substrate. On the conducting line, the polymer jet is spontaneously stacked successively to form a wall-like structure. However, without the conducting line, the electrified jet cannot be precisely stacked because of the mutual coulombic repulsion, which significantly affects its flexibility to produce arbitrary 3D structures. Recently, He et al. [13] presented a solvent-based electrohydrodynamic 3D printing technique that allows fabrication of microscale structures. However, charge accumulation effects on solvent-based electrospinning fibers tend to restrict the number of maximal layers and to prevent the fiber to collect and bond as one coherent structure. Cracks were observed in the printed walls. Hence, solvent-based electrospinning is not considered a suitable additive manufacturing approach.

Near-field melt electrospinning (NFME) is an optimal method to overcome these limitations. For NFME, a molten polymer jet is ejected from the needle tip and stabilized in the near-field region (several millimeters) subjected to an external high voltage. Then the molten jet is collected in a defined pattern on the substrate and solidified. Several works have been done to fabricate microscale 3D structures using melt electrospinning. Brown et al. [14] demonstrated the printing of 3D lattice structures using conventional melt electrospinning; however, the fibers were only interwoven with each other and not bonded as one coherent structure due to the large needle-to-collector distance. The fibers were solidified before reaching the collecting plate, which made them hard to merge into a single structure. They fabricated the QUT IHBI logo using melt electrospinning writing. The fiber diameter was approximately 20 μm [14] due to the large applied voltage. The size limitation in the deposition resolution restricted the printing of microscale structures. Hochleitner et al. [15] fabricated interwoven scaffolds with submicron filaments using melt electrospinning. The breaks

¹Corresponding author.

Contributed by the Manufacturing Engineering Division of ASME for publication in the JOURNAL OF MICRO- AND NANO-MANUFACTURING. Manuscript received June 14, 2017; final manuscript received August 21, 2017; published online September 27, 2017. Assoc. Editor: Yayue Pan.

were observed between the deposited layers; in addition, fiber sagging occurred with the increase in the wall height, which corresponded to a coarse surface finish. It was suspected to be caused by the variation of the temperature and electric field between the needle and the collecting surface.

In this study, we demonstrated for the first-time microscale 3D printing of various 3D thin-wall structures via NFME, including freestanding single walls, double walls, rectangular walls, star-shaped structures, and curved wall structures with a minimal wall thickness less than $5\ \mu\text{m}$. The unique capabilities of proposed process of near-field melt electrospinning are two-fold. (1) Compared with the conventional melt-electrospinning, the proposed near-field concept significantly reduces the applied external voltage and the needle-to-collector distance. It helps to reduce the fiber diameter from $20\text{--}50\ \mu\text{m}$ to $1\text{--}2\ \mu\text{m}$. The reduced deposition distance helps to eliminate the whipping phenomenon for controlled deposition of the spinning jet. (2) Compared with the solvent-based near-field electrospinning, the melt electrospinning utilizes the attraction force between the deposited molten layers and the later arriving fibers to achieve a self-assembly effect. It also eliminates the jet wobbling and stabilizes the ejection point of the jet on the Taylor cone. Through optimization of the parameters of NFME process (electric field strength, collector moving speed, and needle-to-collector distance), poly (ϵ -caprolactone) (PCL) fibers with a minimal fiber diameter of less than $5\ \mu\text{m}$ are stably generated and stacked and fused into 3D thin-wall structures with an aspect ratio of more than 60, which shows the feasibility of translating NFME into a viable high-resolution and low-cost microscale 3D printing technology.

Experimental Setup

Poly (ϵ -caprolactone), with a molecular weight of 80,000 and a melting point of 60°C , was chosen as the material owing to its good biological property and high thermal stability. The NFME platform was schematically shown in Fig. 1. Poly (ϵ -caprolactone) powder was loaded into a 1.5 ml glass syringe fitted with a needle of gauge 26 (inner diameter of $260\ \mu\text{m}$). A proportional-integral-derivative regulated electrical heating system was adopted to ensure that the molten polymer was kept at a stable temperature. A precision syringe pump (Harvard apparatus, remote infuse/withdraw PHD ULTRA syringe pump, Holliston, MA) was used to dispense the molten polymer at a feed rate of $10\ \mu\text{L}/\text{h}$. A precision high voltage supplier (Stanford Research System, Inc., Sunnyvale, CA) was adopted to guarantee the stability of the electrospinning process, the voltage resolution is 1 V, the output ripple (root-mean-square) is less than 0.002% of the full scale (5000 V), the stability is 0.01% per hour. High voltages were applied to the needle tip. A silicon wafer was served as the collector. The collector

was mounted on a programmable X–Y stage (ALIO Industries, Inc., Arvada, CO). The needle and electrical heating system were mounted on a Z-axis stage (ALIO Industries, Inc.). The stage resolution in the X-, Y-, and Z-axes is $1\ \mu\text{m}$, respectively. The stage is controlled by a software-based machine controller (ACS Motion Control, Migdal Ha-Emek, Israel) with the motion capabilities including point-to-point, linear, circular, helical, and spherical interpolations. A microscopic camera (Point Grey Research) was used to monitor and record the NFME process. The whole setup was stationed on a granite table. The experiment was carried out at room temperature and atmospheric pressure.

To initialize the NFME process, the high voltage supplier was adjusted to a predefined value and the molten polymer was dispensed at a constant rate. Minimizing the whipping phenomenon and obtaining thin electrospun fibers are the most critical issues to achieve precise printing of microscale thin-wall structures. In near-field melt electrospinning, when the needle-to-collector distance is fixed, the decrease in the applied voltage will result in a decrease in the collected fiber diameter but an increase in the whipping phenomenon; when the applied voltage is fixed, the decrease in the needle-to-collector distance will result in an increase in the collected fiber diameter but a decrease in the whipping phenomenon. So, our purpose is to find the minimal fiber diameter condition with good printing resolution. Near-field melt electrospinning process parameters (electric field strength, collector moving speed, and needle-to-collector distance) were systematically optimized to achieve a stable ultrafine polymer jet and deposition of 3D microscale thin-wall structures. The optimization process is described as follows: A set of voltage values from 1600 V to 2400 V with a step size of 200 V and another set of needle-to-collector distance values from 0.5 mm to 2.5 mm with a step size of 0.5 mm were adopted to form 25 pairs of process parameter combinations as shown in Fig. 2. All the combinations can be divided into five regions as shown in the figure. (1) In the top left region, where both the applied voltage and needle-to-collector distance are small, the whipping phenomenon will be significant that the deposited fibers could hardly form 3D structures. (2) In the top right region, where the applied voltage is high but the needle-to-collector distance is small, the electric breakdown will occur due to the large electric field intensity. (3) In the bottom left region, where the applied voltage is low but the needle-to-collector distance is large, the electrospinning process cannot be initiated due to the insufficient electric field intensity. (4) In the bottom right region, where both the applied voltage and needle-to-collector distance are large, the distortion phenomenon will be severe due to the increased needle-to-collector distance. (5) The region in the middle of Fig. 2 is then the optimal parameter condition for a stable electrospinning process. The collector moving speed was adjusted to be equal to the fiber ejection

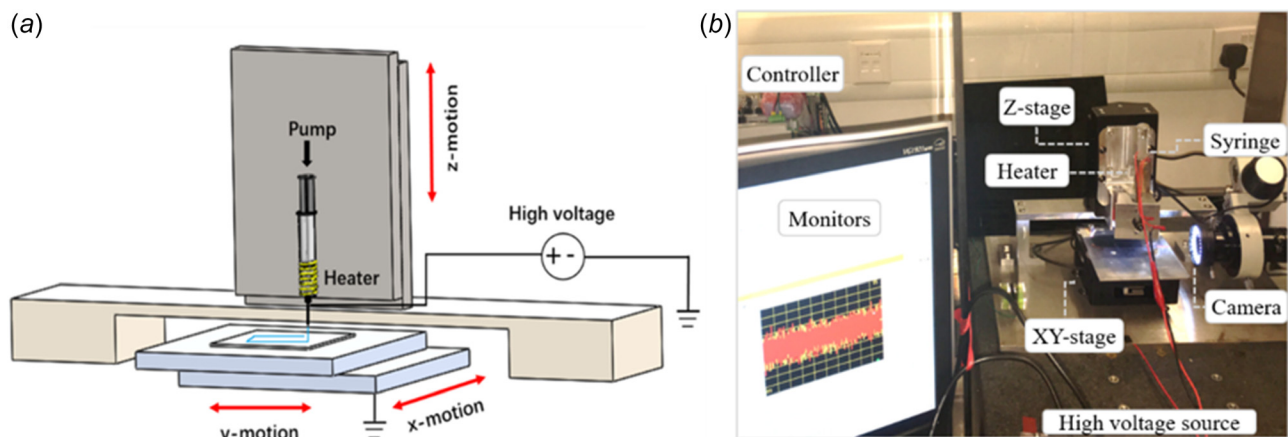


Fig. 1 NFME platform: (a) schematic illustration and (b) photograph of the actual setup

h_t (mm) \ V	1600	1800	2000	2200	2400
0.5					
1.0					
1.5					
2.0					
2.5					

Fig. 2 Parameter optimization for applied voltage and needle-to-collector distance

velocity at 15 mm/s. The optimal experimental condition was determined to be as follows: applied voltage of 2 kV; needle-to-collector distance of 1.5 mm; collector moving speed at 15 mm/s. Various thin-wall structures were fabricated by controlling the collector moving trajectories according to user-defined programs.

Results and Discussion

Fabrication of Single-Wall Structures. The collector moving trajectory for fabricating a single-wall structure is illustrated in Fig. 3. The turning loop will prevent the stagnation point on the trajectory, which will inhibit the whipping motion and improve the jet stability. The result of a single-wall structure was obtained by stacking the PCL fibers in a layer-by-layer manner for 200 layers. The top and perspective views of the wall structure are shown in Figs. 4(a) and 4(b). The measured height and thickness of the free-standing wall were 300 μm and 5 μm , respectively. The free-standing single wall achieved an aspect ratio of more than 60. In order to keep a stable electric field strength or a constant needle-to-collector distance, the syringe mounted on the Z-axis was lifted by a small distance for each cycle of path. Otherwise, the quality of the side surface will not be uniform with the increasing wall height. The fabricated single wall had good strength and could be easily detached from the substrate without any damage. The side view of the detached single wall was shown in Fig. 4(c). It can be seen that the PCL fibers were well bonded together, forming a smooth side surface. The result demonstrated here could motivate a new way to fabricate ultrathin fiber films, which is challenging to be achieved by other traditional methods.

Fabrication of Dual-Wall Structures. Besides single-wall structures, dual-wall structures were investigated in this study for their self-supporting properties even after being removed from the substrate. Two kinds of dual-wall structures were fabricated as shown in Fig. 5. First, we demonstrated the successful printing of two straight walls of 60 layers with a small gap of 100 μm

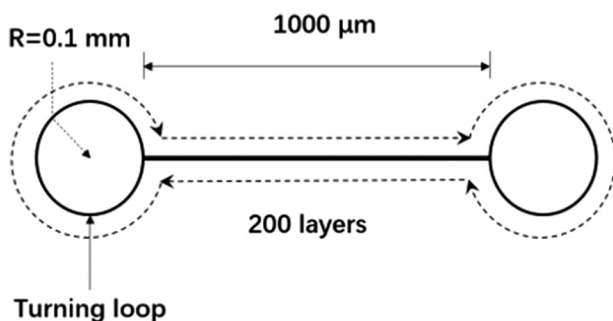


Fig. 3 Schematic of collector moving trajectory for deposition of a single-wall structure

between them. The results are plotted in Figs. 5(a) and 5(b). Sagging could be clearly observed in Fig. 5(b) at the corner, which could be attributed to the large variation of the collector moving speed. We found that dual-wall structures with smaller gaps were hard to be fabricated because of the mutual coulombic repulsion between the bilateral walls. Besides straight walls, the precise stacking of fibers with curved features is also significant for complex structure printing. Based on this concept, an oval-shaped dual-wall structure was fabricated by depositing PCL fibers for 60 layers as shown in Fig. 5(c). The gap between the two straight walls and the circular diameter were both 2 mm. Due to the large turning circle, the speed variation was small; thus, no sagging was observed. Scanning electron microscope (SEM) images of the side surface on the straight and curved paths are shown in Figs. 5(d) and 5(e). The wall height was measured to be 303 μm . Magnified views on the curved walls of 250 \times , 1000 \times , 4000 \times , and 10,000 \times are demonstrated in Figs. 5(f)–5(h). The fabricated walls showed good surface quality with strong bonds between fibers.

Fabrication of Thin-Wall Structures With Complex Geometry.

To further demonstrate the capability of fabricating 3D thin-wall structures with complex geometry using NFME, more results involving different geometry are shown in Fig. 6. Figure 6(a) is the SEM image of a star-shaped thin-wall structure. The fibers were layered 50 times to reach a wall height of 100 μm . However, as shown in Figs. 6(b) and 6(c), the surface quality was not as

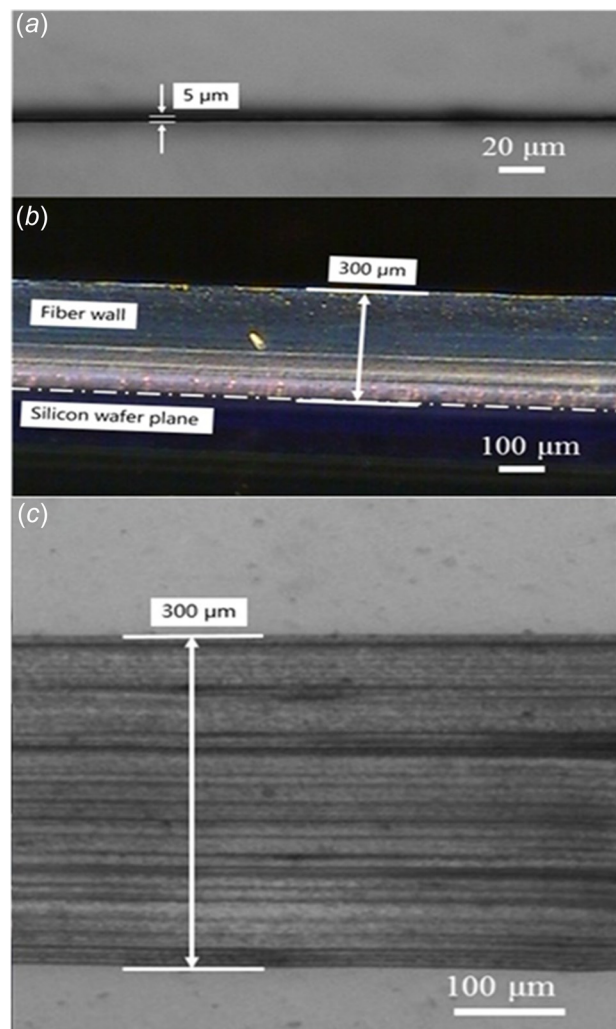


Fig. 4 A freestanding single wall structure fabricated by NFME: (a) top view, (b) perspective view, and (c) side view

good as the previous samples. This might be due to the interweaving of the printed fibers, resulting in the height variation during deposition at the intersection points. As shown by the SEM measurement shown in Fig. 6(d), fiber sagging occurred at the intersection positions, where charges were accumulated much more than other locations. Therefore, larger repulsive force due to residual charges was more significant, which deteriorated the jet stability when the jet was passing through these intersections.

Annular walls with straight and sloped side surfaces in the vertical direction were fabricated as shown in Figs. 6(e) and 6(f), respectively. The actual collector trajectories were following a rectangular tool path, but due to the limited acceleration ability of the X-Y stage, the actual tool path was curved at the four straight corners. The straight annular wall was layered 100 times with the same tool trajectory of a 2 mm × 2 mm rectangular. The wall height was measured to be 550 μm. The sloped annular wall was deposited by: (1) first depositing 50 layers of rectangular loops of 4 mm × 4 mm and (2) then depositing 500 layers of inner rectangular with a decreasing edge length. For each tool path, the rectangular trajectory was shifted inward by 0.5 μm to print a sloped annular wall. The measured height of the overall structure was 2 mm. A sloped wall with a slope angle of 82 deg and an aspect ratio of 400 has been achieved in this sample. Lastly, a letter-K-shaped thin-wall structure is demonstrated in Figs. 6(g) and 6(h).

These results indicate the feasibility of direct writing of complex thin-wall structures using NFME.

Discussion on the Experimental Results. According to the theoretical model derived by Dasdemir et al. [16], the electrostatic force that results in the stretch of the melt electrospinning jet was defined as

$$f_e = \frac{e_t V}{h_t} \quad (1)$$

where f_e is the electrostatic force, e_t is the jet charge, V is the applied voltage, and h_t is the distance between the needle and the collector. Based on this model, the electrostatic force is proportional to the applied voltage and inversely proportional to the needle-to-collector distance. In the near field of the electrospinning jet (very small distance below the spinneret), sufficient electrostatic force can be obtained by a relatively low voltage to initiate the jet ejection.

To achieve precise printing of microscale thin-wall structures, minimizing the whipping phenomenon and obtaining thin electrospun fibers are the most critical issues, which determine the printing resolution and the minimal feature size. As mentioned before, when the needle-to-collector distance is reduced to several millimeters, the whipping phenomenon could be suppressed efficiently

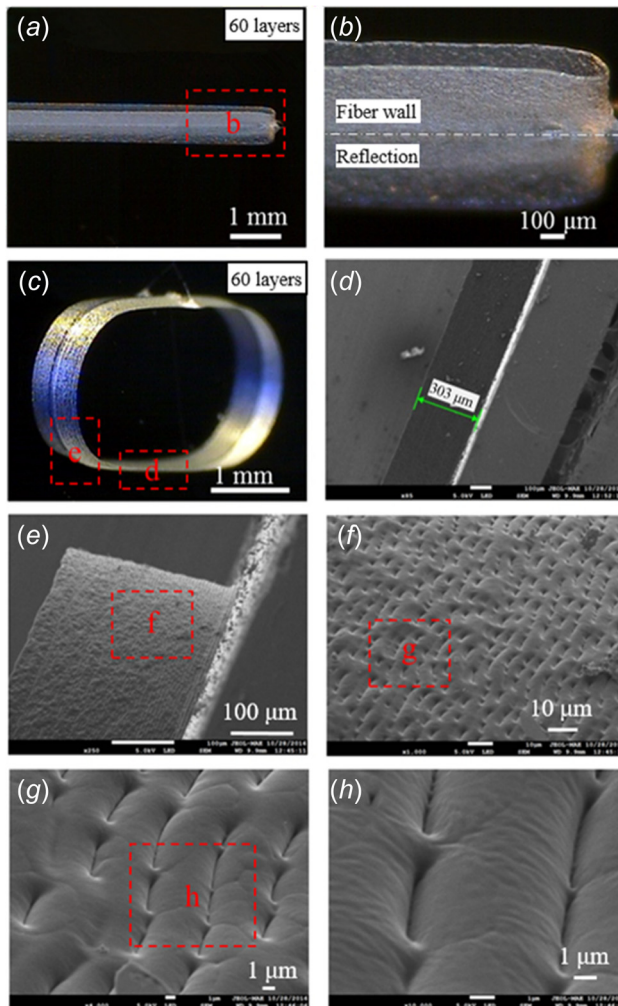


Fig. 5 Fabricated dual wall structures: (a) and (b) dual wall structure with a small gap of 100 μm; (c) dual wall structure with a larger gap of 2 mm; SEM images of: (d) the straight wall and (e) the curved wall; and (f)–(h) SEM images of magnified view of the curved wall shown in (e)

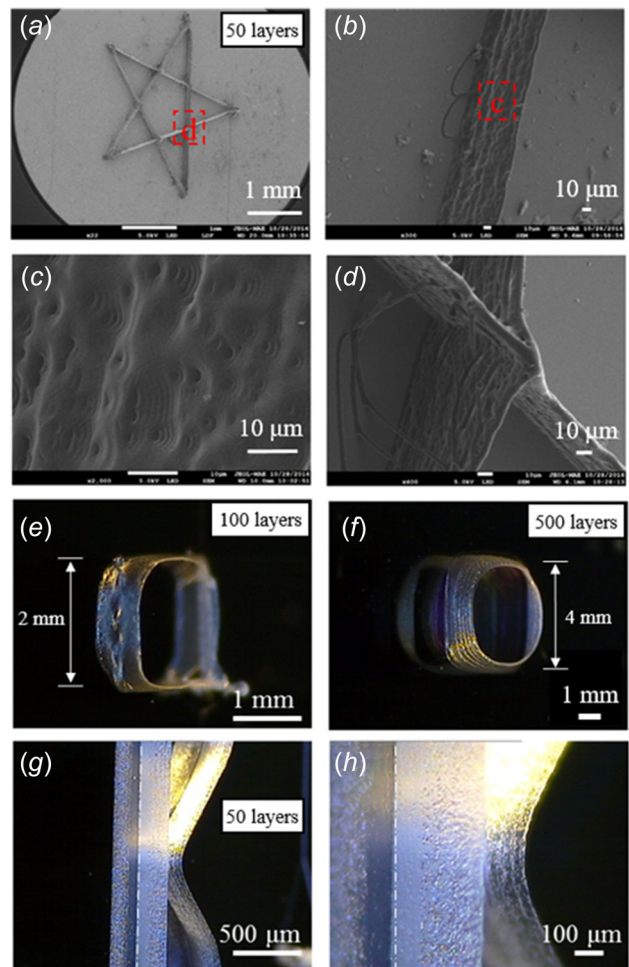


Fig. 6 Fabricated thin-wall structures with complex geometry: (a) SEM image of a star-shaped structure; (b) and (c) SEM images of the side surfaces of (a); (d) fiber sagging at the intersection position; annular walls with (e) straight and (f) sloped side surfaces; (g) and (h) letter-K-shaped thin wall

owing to the low applied voltage. The overall decrease in the repulsive force between the charges accumulated on the electrospinning jet helps to improve the jet stability.

The electrospun fiber diameter is affected by many parameters, including the electric field strength, heating temperature, pumping rate, collector speed, etc. Deng et al. [17] showed that when the needle-to-collector distance, h_t , was fixed and the applied voltage, V , was increased, the diameter of low-density polyethylene fibers decreased pronouncedly due to the larger electrostatic force, f_e , which contributed to the stretching of the polymer jet during the landing path. In the near-field case, however, the higher applied voltage will lead to thicker fibers. This phenomenon indicates that, when the needle-to-collector distance is too short, the melt jet does not have sufficient time for stretching before reaching the collector; and the fiber diameter is mainly determined by the jet ejection speed. Therefore, in near-field melt electrospinning, the decrease in the applied voltage will result in the decrease in the collected fiber diameter. In addition, a higher heating temperature and lower flow rate would both contribute to the smaller fiber diameter by reducing the jet ejection speed.

Another highlight of NFME is its short needle-to-collector distance, which contributes to the bonding of thin-wall structures. Since a shorter needle-to-collector distance leads to a shorter jet in-flight time, the molten jet does not have sufficient time to fully solidify before reaching the collector. Furthermore, a self-assembly effect for stacking single-fiber wall structures can be achieved in NFME. A high electric field intensity can polarize dielectric materials (like PCL), which causes accumulation of negative charges on the upper part of the deposited fiber wall. Meanwhile, the upcoming polymer jet is electropositive, since electrons can cross the boundary between the metal electrode and fluid by a quantum tunneling mechanism [18] during the electrospinning process. Therefore, attraction force is more significant between the deposited fiber and upcoming polymer jet, which facilitates the self-assembly effect, while in solution-based electrospinning, the repulsion force due to the accumulated residual charges on the deposited fibers will dominate the interaction between the upcoming fibers and the deposited structure, which will deteriorate the jet stability and prevent self-assembly.

Conclusions

In conclusion, a near-field melt electrospinning process platform was developed and the feasibility of employing NFME to print microscale thin-wall structures with high-resolution was verified. Through optimization of the NFME process parameters (electric field strength, collector moving speed, and needle-to-collector distance), ultrafine PCL fibers were stably produced and precisely stacked and fused into 3D thin-wall structures with an aspect ratio of more than 60. Various 3D thin-wall structures (single wall, dual wall, annular wall, star-shaped wall and curved wall structures) in microscale with the minimal wall thickness of about $5\ \mu\text{m}$ were fabricated and demonstrated. These results indicate that NFME can be potentially transformed to a high-resolution, low-cost, and flexible microscale 3D printing process.

Funding Data

- Research Grants Council, University Grants Committee (Grant No. ECS 24201816).
- Shun Hing Institute of Advanced Engineering (Grant No. BME-p6-16).

References

- [1] Garlapati, S. K., Baby, T. T., Dehm, S., Hammad, M., Chakravadhanula, V. S. K., Kruk, R., Hahn, H., and Dasgupta, S., 2015, "Ink-Jet Printed CMOS Electronics From Oxide Semiconductors," *Small*, **11**(29), pp. 3591–3596.
- [2] Rutz, A. L., Hyland, K. E., Jakus, A. E., Burghardt, W. R., and Shah, R. N., 2015, "A Multimaterial Bioink Method for 3D Printing Tunable, Cell-Compatible Hydrogels," *Adv. Mater.*, **27**(9), pp. 1607–1614.
- [3] Sun, K., Wei, T. S., Ahn, B. Y., Seo, J. Y., Dillon, S. J., and Lewis, J. A., 2013, "3D Printing of Interdigitated Li-Ion Microbattery Architectures," *Adv. Mater.*, **25**(33), pp. 4539–4543.
- [4] Li, W. J., Laurencin, C. T., Catterson, E. J., Tuan, R. S., and Ko, F. K., 2002, "Electrospun Nanofibrous Structure: A Novel Scaffold for Tissue Engineering," *J. Biomed. Mater. Res.*, **60**(4), pp. 613–621.
- [5] Williams, J. M., Adewunmi, A., Schek, R. M., Flanagan, C. L., Krebsbach, P. H., Feinberg, S. E., Hollister, S. J., and Das, S., 2005, "Bone Tissue Engineering Using Polycaprolactone Scaffolds Fabricated Via Selective Laser Sintering," *Biomaterials*, **26**(23), pp. 4817–4827.
- [6] Jansen, J., Melchels, F. P., Grijpma, D. W., and Feijen, J., 2008, "Fumaric Acid Monoethyl Ester-Functionalized Poly (D, L-Lactide)/N-Vinyl-2-Pyrrolidone Resins for the Preparation of Tissue Engineering Scaffolds by Stereolithography," *Biomacromolecules*, **10**(2), pp. 214–220.
- [7] Huttmacher, D. W., Schantz, T., Zein, I., Ng, K. W., Teoh, S. H., and Tan, K. C., 2001, "Mechanical Properties and Cell Cultural Response of Polycaprolactone Scaffolds Designed and Fabricated Via Fused Deposition Modeling," *J. Biomed. Mater. Res., Part A*, **55**(2), pp. 203–216.
- [8] Ko, S. H., Chung, J., Hotz, N., Nam, K. H., and Grigoropoulos, C. P., 2010, "Metal Nanoparticle Direct Inkjet Printing for Low-Temperature 3D Micro Metal Structure Fabrication," *J. Micromech. Microeng.*, **20**(12), p. 125010.
- [9] Strano, G., Hao, L., Everson, R. M., and Evans, K. E., 2013, "Surface Roughness Analysis, Modelling and Prediction in Selective Laser Melting," *J. Mater. Process. Technol.*, **213**(4), pp. 589–597.
- [10] Muller, P., Mognol, P., and Hascoet, J.-Y., 2013, "Modeling and Control of a Direct Laser Powder Deposition Process for Functionally Graded Materials (FGM) Parts Manufacturing," *J. Mater. Process. Technol.*, **213**(5), pp. 685–692.
- [11] Dalton, P. D., Vaquette, C., Farrugia, B. L., Dargaville, T. R., Brown, T. D., and Huttmacher, D. W., 2013, "Electrospinning and Additive Manufacturing: Converging Technologies," *Biomater. Sci.*, **1**(2), pp. 171–185.
- [12] Lee, M., and Kim, H.-Y., 2014, "Toward Nanoscale Three-Dimensional Printing: Nanowalls Built of Electrospun Nanofibers," *Langmuir*, **30**(5), pp. 1210–1214.
- [13] He, J., Xu, F., Cao, Y., Liu, Y., and Li, D., 2016, "Towards Microscale Electrohydrodynamic Three-Dimensional Printing," *J. Phys. D: Appl. Phys.*, **49**(5), p. 055504.
- [14] Brown, T. D., Dalton, P. D., and Huttmacher, D. W., 2011, "Direct Writing by Way of Melt Electrospinning," *Adv. Mater.*, **23**(47), pp. 5651–5657.
- [15] Hochleitner, G., Jüngst, T., Brown, T. D., Hahn, K., Moseke, C., Jakob, F., Dalton, P. D., and Groll, J., 2015, "Additive Manufacturing of Scaffolds With Sub-Micron Filaments Via Melt Electrospinning Writing," *Biofabrication*, **7**(3), p. 035002.
- [16] Dasdemir, M., Topalbekiroglu, M., and Demir, A., 2013, "Electrospinning of Thermoplastic Polyurethane Microfibers and Nanofibers From Polymer Solution and Melt," *J. Appl. Polym. Sci.*, **127**(3), pp. 1901–1908.
- [17] Deng, R., Liu, Y., Ding, Y., Xie, P., Luo, L., and Yang, W., 2009, "Melt Electrospinning of Low-Density Polyethylene Having a Low-Melt Flow Index," *J. Appl. Polym. Sci.*, **114**(1), pp. 166–175.
- [18] Collins, G., Federici, J., Imura, Y., and Catalani, L. H., 2012, "Charge Generation, Charge Transport, and Residual Charge in the Electrospinning of Polymers: A Review of Issues and Complications," *J. Appl. Phys.*, **111**(4), p. 044701.